crystals

MDPI

Article

Self-Organization of Micro- and Nanosystems in the Form of Patterns

Vyacheslav Perekrestov [1], Anna Kornyushchenko [1,2,*], Yuliia Kosminska [1], Maksym Kubakh [1] and Gerhard Wilde [2]

[1] Laboratory of Vacuum Nanotechnologies, Sumy State University, 40007 Sumy, Ukraine; v.perekrestov@phe.sumdu.edu.ua (V.P.); y.kosminska@phe.sumdu.edu.ua (Y.K.); m.kubakh@ksu.sumdu.edu.ua (M.K.)

[2] Institute of Materials Physics, University of Muenster, 48149 Muenster, Germany; gwilde@uni-muenster.de

* Correspondence: korniusg@uni-muenster.de or ganna.korniushchenko@fulbrightmail.org

Abstract: In this work, the peculiarities of self-organization of patterned micro- and nanosystems under near-equilibrium condensation conditions were consistently considered. The criteria for stationarity of near-equilibrium condensation were introduced, and interrelations between the condensate local growth kinetics and the corresponding local technological parameters were described. Dissipative self-organization of small supersaturations in physically and chemically active medium-condensate systems were compared. The effectiveness of the unification of dissipative self-organization of small supersaturations and conservative self-organization of patterned micro- and nanosystems formation was shown, which forms the basis of a new concept of complete self-organized systems.

Keywords: nucleation; self-organization; nanosystems; patterns

1. Introduction

The process of materials fabrication at the nanoscale level increasingly depends on the atoms' self-assembly into organized low-dimensional systems using the "bottom-up" principle. Currently, there are two approaches to the formation of materials with micro- and nanosized structural elements: the first being the "top-down", and the second being the "bottom-up". Using a top-down approach, the bulk material is reduced in size into micro- and nanoparticles which can then be used to create layers with the desired morphology. At the same time, using the "bottom-up" approach, the particles of matter are manipulated at the atomic or molecular level in order to form a material with the required properties.

Well-known "bottom-up" examples of micro- and nanopatterned structures formation include the growth of epitaxial graphene, nanotubes, fullerenes, quantum dots arrays, different heterosystems, and other materials having quantum-dimensional features. Considerable interest of researchers is dedicated to the development of new strategies for the porous micro- and nanosystem synthesis because of a wide range of possible applications, for example, in bio and gas sensors [1–7], catalysts [8–12], as battery electrodes [13–16], fuel cell membranes [17,18], etc. An important process in nanosystem fabrication is patterning, which is typically used within film condensation processes. The presence of elements of self-organization in the corresponding deposition technology is indicated by the formation of structural repetition in a certain order and coordinated sizes of structural elements (patterns) during the deposition of a substance. It is assumed that self-assembly and self-organization processes will play increasingly important roles in pattern formation at the nanoscale.

The effectiveness of processes of self-organization can be illustrated by the example of matrix biosynthesis of proteins and subsequent formation of their tertiary structure, as well as by other biomacromolecules formation, which is an essential precondition for the functioning of living organisms. Along with this, it is difficult to imagine the creation of

check for updates

Citation: Perekrestov, V.; Kornyushchenko, A.; Kosminska, Y.; Kubakh, M.; Wilde, G. Self-Organization of Micro- and Nanosystems in the Form of Patterns. *Crystals* **2024**, *14*, 953. https://doi.org/10.3390/cryst14110953

Received: 8 October 2024
Revised: 21 October 2024
Accepted: 25 October 2024
Published: 31 October 2024

Copyright: © 2024 by the authors. Licensee MDPI, Basel, Switzerland. This article is an open access article distributed under the terms and conditions of the Creative Commons Attribution (CC BY) license (https://creativecommons.org/licenses/by/4.0/).

an artificial living cell in which the selective formation of extremely complex interrelated physical and chemical processes of various proteins and cellular structures would be controlled from the outside. Even quite straightforward, as compared to processes in living nature, molecular beam epitaxy technology with artificial feedback control system between condensate structure formation mechanism and the technological parameters is quite costly and technologically complex. For these reasons, the development of self-organized systems that are capable of reproducible nanosystem formation in the form of patterns attracts considerable research attention [19,20].

Self-organization is an internal process that leads to the formation of a spatial, temporal, spatiotemporal, or functional structure in a system without an influence of external control factors [21,22]. An example of an external control factor affecting patterning could be the usage of membranes as templates for the formation of an ordered system of nanoislands [23]. Nowadays, two concepts of self-organization processes are best known, i.e., dissipative and conservative processes. The main principles of dissipative self-organization have been formulated by H. Haken, I. Prigogin, G. Nicolis, and M. Feigenbau. In this case, the process takes place under non-equilibrium conditions, and various parameters of the system are nonlinearly interrelated. The system consists of large number of elements that take part in the process. Moreover, there is an exchange of both energy and the matter between the system and the external environment; in other words, the system is open [24–29]. The presence of a control parameter that determines the interaction type of the system constituent elements is also a required precondition, evidencing that the system is dissipative [24]. As a result, at the moment when the processes parameters reach some critical value, there is a spontaneous decrease in the entropy, which brings the system into the ordered state. At the same time, a rather important variant of dissipative self-organization is the formation of a functional structure that is stable over time, which can become the technological base for the self-assembly of various nanoobjects. An example of such functional structures is warm-blooded living organisms in which the self-organization of a constant temperature, substances concentration, and other parameters continuously takes place, which are absolutely necessary for biopolymers and cellular structures' self-assembly under near-equilibrium thermodynamic conditions.

Unlike dissipative self-organization, in conservative or closed systems, according to Zh.-M. Len, the process occurs under thermodynamically near-equilibrium conditions and provides the assembly of supramolecular architectures from individual units [30–33]. At the same time, as it will be shown later in the work, nonlinear interrelation between physical and chemical processes also takes place in the case of conservative self-organization, similar to the dissipative one. It should be noted that classical ideas about the dissipative self-organization of supramolecular ensembles have been described for noncovalent bonds on the intermolecular level [30–33]. At the same time, the possibility of nanosystem self-assembly based on any other type of chemical bonds has not been physically disapproved. It should also be pointed out that perfectly isolated conservative systems do not exist. For example, living cells exchange matter and energy with the environment, from which they are clearly separated by cell membranes. At the same time, local conditions are created and maintained in the intracellular environment in which various structures self-assemble, such as three-dimensional protein structures, hierarchical DNA structures, polymer elements of the cytoskeleton, etc. All these processes occur under conditions close to thermodynamic equilibrium and therefore the self-organization is a necessary precondition for living nature existence [34]. This example indicates the high efficiency of interrelated processes inherent to conservative and dissipative self-organization. Thus, similarly to conservative self-organization, the processes of patterned nanosystem self-assembly also occurs under close to thermodynamic equilibrium conditions. At the same time, both supramolecules self-organization and metal nanosystems' conservative self-assembly [33,34] lead to a decrease of the Gibbs free energy to the minimum value and the appearance of a new system quality that varies from just the total sum of its component properties. Therefore, a conclusion can be made that the self-organization processes by Zh.-M. Len and self-

assembly of patterned nanosystems have a common physical basis [35–37]. Based on this, from now on, we define the term conservative self-organization of nanosystems as analogue to self-assembly expression.

Taking into account the above, one could suggest that dissipative and conservative self-organization forms are very complexly interrelated in living nature, originating, in this manner, as extremely efficient systems of complete self-organization. This approach can be extrapolated onto the processes of artificial objects' nanofabrication having a non-living nature. With this in mind, in this paper, the nucleation peculiarities during condensation under near-equilibrium conditions, which are necessary elements of conservative self-organization, are considered for the first time. The required technological conditions are created by means of deposition from the vapor phase and simultaneous plasma action onto the growth surface. In addition to that, nonlinearly interconnected technological parameters are analyzed during low relative supersaturations self-organization through dissipative mechanism in technological systems based on plasma and in systems that use chemically active media. Finally, the definition of complete self-organization systems is introduced, and prospects of their application for the formation of patterned nanosystems are given.

The main aim of the work consists in the theoretical and experimental study of the peculiarity of the combination of dissipative self-organization of depositing vapors ultralow supersaturations with elements of conservative self-organization of micro- and nanopatterned condensates under these conditions. In other words, the goal of the work is to demonstrate the possibility of a system of complete self-organization implementation when forming nanosystems in the form of patterns based on a combination of dissipative and conservative self-organization. With this aim, concepts of conservative and dissipative self-organization, mechanisms of condensate nucleation at high and low supersaturations, nucleation processes under near-equilibrium condensation conditions, and simultaneous action of plasma onto the growth surface are consistently considered in the work.

2. Materials and Methods

2.1. Nucleation Processes Under Near-Equilibrium Conditions and Simultaneous Action of an Active Medium

The main technological parameters that influence the nanostructure formation mechanism from a vapor phase under an influence of an active medium onto the growing condensate include temperature of the growth surface T_s; the depositing flow of substance approaching the growth surface J_c; the condensing flow J_s (for near-equilibrium condensation $J_s = kJ_c$, $0 < k \ll 1$); the flow of particles acting onto the growth surface J_p; the relative supersaturation ξ of condensing vapors; depositing vapor pressure P_c; the equilibrium pressure P_e. At the initial stage of the self-organization process, these non-linearly interdependent technological parameters change over time. An active medium affecting the growth surface during condensation process could be the action of plasma particles or chemically active species. In order to obtain condensates with reproducible characteristics, some technological parameters must be constant over time. The latter include the working gas pressure P_i, that is, the pressure of Ar ions, which sputter the target material in the case of magnetron sputtering; the partial pressure of the residual chemically active gases P_z in the vacuum chamber; various geometric characteristics of the technological system; the substrate material; and the surface structure. It is necessary to point out that these parameters indirectly affect the main technological parameters.

During the vapor transition into a condensed state at near-thermodynamic-equilibrium conditions, the chemical potential difference $\Delta\mu$ between the vapor and the condensed phases should have a relatively small value. For this case, according to [38]:

$$\Delta\mu \approx k_b T_c \frac{P_c - P_e}{P_e} \equiv k_b T_c \xi, \quad (1)$$

where k_b is Boltzmann's constant. Thus, under the condition of dissipative self-organization of time-invariant technological parameters, a small value of relative supersaturation ξ can represent a criterion of approaching to thermodynamic equilibrium. At the same time, the equilibrium vapor pressure is determined by the ratio [39]:

$$P_e = A(T_c)\exp\left(-\frac{E_d}{k_b T_c}\right), \quad (2)$$

where $A(T_c) = exp(\alpha + \beta T_c + \gamma/T_c)$; α, β, and γ are the characteristic constants of the deposited material; E_d is the energy of atoms desorption from the growing surface. Analyzing Relations (1) and (2), a conclusion could be made that in order to achieve close-to-equilibrium condensation conditions, it is necessary to increase T_c, decrease the deposited flow J_c or current vapor pressure above the growth surface P_c, and to reduce the desorption energy E_d. Earlier, it has been shown [40,41] that the influence of plasma directly onto the growing nanosystem surface determines the decrease of the energy of the adatoms desorption E_d to some effective value:

$$E_{df} = E_d - \delta E, \quad (3)$$

where δE is a stochastic value of desorption energy reduction, which has an average value $\langle \Delta E \rangle$. At the same time, the calculations show [42] that for the plasma–condensate system the following ratio holds true:

$$\langle \Delta E \rangle = k_b T_c \ln\left(1 + \frac{\Delta S(T_p - T_c)}{\Delta\Omega \exp(\alpha + \beta T_c + \gamma/T_c)} \exp\left(\frac{E_d}{k_b T_c}\right)\right), \quad (4)$$

where $\Delta\Omega = \Omega_v - \Omega_c$ and Ω_v and Ω_c are the volumes occupied per unit mass of a particle in vapor and condensate phase, respectively; $\Delta S = S_v - S_c$ and S_v and S_c are the entropies of vapor and condensate states, respectively; T_p is the temperature of plasma.

Analyzing to Relations (1)–(4), one may conclude that the growth of the plasma temperature value T_p determines the approach of the condensation process to the equilibrium conditions, and in the case when the temperature of the plasma approaches the growth surface temperature T_c, then $\langle \Delta E \rangle \to 0$. From a physical standpoint, this process is determined by a decrease in the coefficient of thermal accommodation of adatoms thermalized in the plasma [43–45], having initially increased energies [46,47]. Moreover, it is necessary to take into account that there is a direct energy transfer from plasma particles to adatoms. These factors increase the probability of re-evaporation, which increases in turn the equilibrium pressure over the growth surface and, accordingly, decreases $\Delta\mu$. On the basis of Relation (1), the following ratio can be easily obtained:

$$P_c = P_e(\xi + 1), \quad (5)$$

which confirms the possibility of increase in P_c and, as a result, in the condensing flow J_s by increasing P_e and keeping a small time-constant value of ξ. Since the majority of metals and semiconductors, even at significantly high temperatures, have rather small values of P_e, the influence of plasma onto the growth surface makes it possible to form nanosystems at low values of $\Delta\mu$ with a high growth rate. To understand the influence of the chemical potential difference fluctuations on the patterned nanosystem formation under conditions close to equilibrium, let us consider a simplified schematic representation of $\Delta\mu$ dependencies on an arbitrary growth surface coordinate x, at high $\Delta\mu_1(x)$ and low $\Delta\mu_2(x)$ values of this parameter, respectively (Figure 1). Such fluctuations in chemical potential differences are caused by local structural and morphological characteristics of the growing surface. At the same time, the mentioned fluctuations are more pronounced at small values of $\Delta\mu$ and when the type of the substrate corresponds to the Volmer–Weber nucleation conditions.

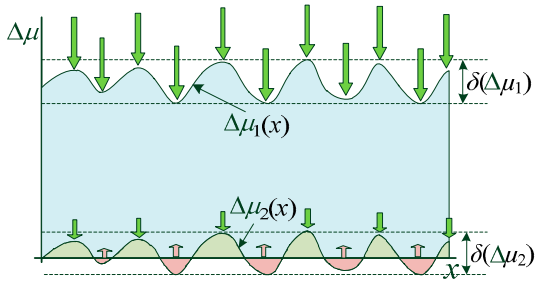


Figure 1. Dependencies of $\Delta\mu_1(x)$ and $\Delta\mu_2(x)$ on the coordinate of the growth surface x, at high and low values of $\Delta\mu$, respectively. Here, $\delta(\Delta\mu_1)$ and $\delta(\Delta\mu_2)$ are maximum values of $\Delta\mu$ fluctuations.

Therefore, in this case, for $\Delta\mu_2(x)$, the relative values of the fluctuations acquire increased values, i.e., according to Figure 1, the following inequality holds true:

$$\frac{\delta(\Delta\mu_2(x))}{\Delta\mu_2(x)} \gg \frac{\delta(\Delta\mu_1(x))}{\Delta\mu_1(x)} \tag{6}$$

Therefore, condensate nucleation and growth was observed only in certain local areas of the substrate surface, where $\Delta\mu_2(x) > 0$ (the green areas in Figure 1). At the same time, usage of single-crystal substrates and near-equilibrium nucleation conditions according to Stranski–Krastanov or Frank–van der Merwe modes would most probably determine the epitaxial growth of continuous thin films, or, in some cases, the growth of graphene [48,49].

Under far-from-equilibrium conditions, i.e., when $\Delta\mu_1(x) \gg 0$, the relative fluctuations of the chemical potential difference are not significant. In this case, the nucleation of the new phase occurs with approximately the same probability, regardless of the value of the x coordinate. In other words, under these conditions, the local features of the growth surface do not have a considerable impact on the condensate nucleation and growth, as a result continuous non-porous films are formed in this case. It is worth mentioning that during the beginning stage of the condensate formation at high supersaturations, the adatoms concentration on the growth surface is quite high. Consequently, periodic fluctuations in the concentration of adatoms cause the formation of the new phase on the substrate surface. In other words, a significant surface concentration of adatoms most likely leads to their accelerated fluctuational joining into a new-phase supercritical nucleus. The phase state of the nuclei is determined by the temperature and pressure of the external environment. For example, when highly supersaturated carbon vapors are deposited, according to the Leypunsky state diagram, a graphite-like phase is always formed. Along with this, it is well known that the condensation of a highly supersaturated metal vapor determines the formation of structurally weakly ordered continuous films. Under the influence of external factors, these structurally disordered thin films can be transformed into a more ordered state. Along with this, at small supersaturation, the number of atoms in the critical nucleus, in accordance with the classical barrier nucleation concept, is determined by the relation [50]:

$$i_c = \frac{a}{ln^2(\xi + 1)} \tag{7}$$

Here, $= \pi\nu(\sigma/k_bT_c)^2/h_v$; ν is the average volume that one atom occupies in the critical nucleus; σ is the specific interface energy of nucleus-substrate interface; h_v is the height of the disk-shaped nucleus. Thus, when ξ decreases, the number of atoms in the critical nucleus rises with a simultaneous reduction of the density of adatoms on the substrate surface. These two tendencies gradually minimize the possibility of the accelerated integration of adatoms into a supercritical nucleus, and at sufficiently small values of ξ, the transition to atom-by-atom incorporation of substance into a subcritical nucleus occurs. On the other hand, processes of atom desorption from unstable subcritical nuclei can lead to their disintegration. At the same time, for some of the most stable nuclei,

fluctuations of positive free energy can lead to overcoming of the activation nucleation barrier [51–58] that initiates the growth of a new phase.

Therefore, the condensation process under conditions when the plasma–condensate system reaches near-equilibrium state is characterized by atom-by-atom fixation of substance into various active centers of the growth surface. Active centers are characterized by a discrete series of desorption energies ($E_{d1} > E_{d2} > \ldots > E_{di} > \ldots > E_{dn}$). The availability of a limited number of active centers on the growth surface with increased energy of chemical bonds for atom-by-atom attachment play an important role during condensate nucleation processes under near-equilibrium conditions. Using (1) and (2), it is easy to obtain the ratio:

$$\frac{P_c \cdot \exp(E_d/(k_b T_c))}{A(T_c)} - 1 = \xi, \tag{8}$$

Analyzing (8), the following conclusion can be made: under the conditions of unchanged P_c, a constant small value of ξ, and increased values of T_c, the atoms can be fixed only on the active centers having increased values of E_{di}, which corresponds to the case when the maximally strong chemical bonds are realized. In other words, for small values of E_{di} and increased T_c, the relative supersaturation can take negative values, which excludes the fixation of adatoms on the corresponding active centers. At the same time, as aforementioned, in the instance of plasma influence onto the growing surface, the energy of desorption decreases to some effective value, which also make those active centers that have low desorption energies ineffective.

At the end of this section, we note that the desorption energy decrease to some effective value can occur not only when a physically active medium, such as plasma, acts onto the growth surface. At the presence of a chemically active medium, like hydrogen, for example, above the carbon growth surface, processes similar to the effects corresponding to the action of plasma can take place. The chemical interaction of hydrogen with carbon adatoms weakly connected to the growth surface can lead to volatile hydrocarbon formation, that are quite easily desorbed from the surface. In this case, we can talk about the effect of a chemically active species onto the growing condensate surface. Moreover, a solution acting onto the growth surface could also act as a chemically active medium. Obviously, the combined action of physically and chemically active species onto the growing condensate makes it possible to reduce the energy of adatoms desorption to the effective value more efficiently and, as a result, according to expression (5), to form nanosystems at low relative vapor supersaturations with an increased condensation rate.

2.2. Criterion of Stationarity of Near-Equilibrium Condensation

In order to form predictable and reproducible nanosystems in the form of patterns with desirable morphology under near-equilibrium, it is crucial to solve the problem of controllability and stationarity of the deposition process. It is a quite challenging technological task, which is complicated by the fact that the process occurs at rather small supersaturations, and it is very difficult to form weak fluxes that are stationary at the same time. Thus, in this case, even fairly small fluctuations of the main technological parameters can lead to significant relative changes of small supersaturation. Moreover, changes of the condensate surface structure and morphology at the local level during its growth can also significantly affect the value of the local small supersaturation. In this regard, the criterion of the stationarity of the condensation process at the local level is determined by the time-invariant critical desorption energy E_{dc} value [41], for which $\xi = 0$. Based on the definition of E_{dc}, the following relation can be derived from (8):

$$E_{dc} = k_b T_c \ln \frac{A(T_c)}{P_c} \tag{9}$$

From a physical point of view, E_{dc} divides the entire spectrum of local desorption energies into two parts. Thus, on active centers for which the condition $E_{di} > E_{dc}$ is fulfilled,

the attachment of atoms occurs with a high probability, and, conversely, under the condition $E_{di} < E_{dc}$, the attachment of atoms on the corresponding active centers is mostly impossible. Based on this, during the condensation of carbon, the simplified purely kinetic conditions for the transition from graphite to diamond, and further, to graphene or carbon nanotubes with a decrease in the supersaturation of the condensed vapor, can be presented as follows: The formation of graphite-like phases is possible under the condition $E_{i(vd)} > E_{dc}$, where $Ei_{(vd)}$ is a set of relatively small desorption energies of carbon atoms on the surface of graphite hexagons. Under these conditions, during more prolonged condensation, a system of hexagons connected with van der Waals forces corresponding to the graphite phase is formed. It should be noted that the formation of a graphite-like phase can be accompanied by the nucleation of diamond phase inclusions [57] because $E_{i(sp^3)} > E_{i(vd)} > E_{dc}$, where $E_{i(sp^3)}$ is the energy of desorption based on sp^3 type of carbon atoms' bonds. Along with this, the necessary prerequisites for the predominant formation of a diamond phase are determined by the inequality $E_{i(sp^3)} > E_{dc} > E_{i(vd)}$, and for epitaxy of graphene or the formation of nanotubes, it is necessary that $E_{i(sp^2)} > E_{dc} > E_{i(sp^3)}$, where $E_{i(sp^2)}$ are the spectra of the desorption energies from active centers of the growth surface formed based on sp^2 carbon bonds. At the same time, it is important to mention that the atom-by-atom assembly of the diamond phase occurs outside the Leypunsky state diagram, which indicates qualitative changes in the condensate structure formation mechanisms during the approach to thermodynamic equilibrium conditions. At the same time, the implementation of stronger chemical bonds determines the reduction of Gibbs free energy. In some cases, such minimization leads to the self-organization of weakly interconnected systems of crystals having identical habitus built on the basis of one type of crystallographic plane for which the strongest chemical bonds of atoms are realized [36,40]. In addition, during long-term condensation, the self-organization of systems of whiskers or interconnected nanowires is possible, which is also determined by the growth of structural elements in the direction of crystallographic planes with highest energies of chemical bonds [59,60].

The local stationarity of condensate growth could be also affected by energy scattering of plasma particles, interacting with the growth surface. Thus, when plasma particles and condensing atoms have rather broad energy spectra, this inevitably increases the dispersion of all effective desorption energy values. As a result of such an increase, the desorption energy spectrum becomes less discrete, which, in turn, reduces the spatially distributed selectivity of the condensate growth. Such a process is not desirable for the formation of nanosystems in the form of patterns. In the case of magnetron sputtering, for example, the energy of the plasma particles can be averaged by increasing the pressure of the inert working gas, which is used to form the flow of ions for target sputtering. At the same time, the calculations show that the working gas pressure should be ~5÷8 Pa, and relative supersaturations should not exceed ~0.1 [41,42].

2.3. Experimental Setup

The operation principle of the sputtering device used for micro- and nanosystems' formation was based on combination of direct current magnetron sputtering and hollow cathode effect and additional influence of plasma onto the surface of growing condensate. The hollow cathode was made entirely from the material to be condensed. In the case of Al, Ti, and Cu layers; formation, metal targets with 99.9% purity were used. For purpose of carbon nanostructures synthesis, acetone vapors were used as a working gas. The schematic device cross-section is represented in Figure 2; it operated under the conditions of the pressure of purified inert gas Ar 4÷8 Pa. The working principle was as follows: At region 4, where the lines of magnetic field B and the electric field E intersected, the prerequisites for the magnetron effect were created. The magnetic field was created by the magnet system 1, and the potential difference of 400 V was applied between anode 2 and cathode 3, resulting in the non-self-sustaining glow discharge.

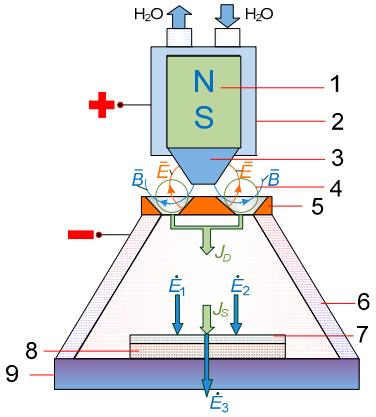


Figure 2. Schematic illustration of the sputtering device: 1—the magnet system; 2—the water-cooled anode; 3—the magnetic guide; 4—the area of crossed electric and magnetic fields; 5—the sputtered part of the cathode; 6—the cathode; 7—the condensate being deposited; 8—the substrate; 9—the base of the cathode [59].

Highly energized Ar ions sputtered the cathode that served as a target in our case. It is necessary to point out that the substance was sputtered mainly from the area at the hollow cathode opening; the erosion zone is denoted by position 5. The plasma density inside the cathode was about one order of magnitude larger than the plasma density of the magnetron discharge. In addition, because of the effect of the hollow cathode, a flow of electrons came out of the volume of the latter, additionally supporting the discharge. As a result, the electron beam coming out of the hollow cathode additionally ionized sputtered atoms, and the ions were accelerated by the electric field in the direction of substrate 8 that was placed inside the cathode.

Moreover, rather high values of the working gas pressure were the used in our case, which defined the diffusion mode of sputtered substance motion and following accumulation inside the hollow cathode to the level at which a low vapors relative supersaturation was observed. At this point, nanosystem 8 started to form on the substrate. Once the technological process reached a stationary operation mode, a constant concentration of sputtered atoms was formed near the opening of the hollow cathode. Figure 2 schematically shows following flows of substance and energy: the depositing flow J_s,; the specific diffusion flow of sputtered atoms to the substrate surface J_d; as well as the specific energy flow $\dot{E}_1$, which was transferred to the growth surface by plasma action; the specific flow of energy $\dot{E}_2$ due to the complete thermal accommodation of condensed atoms; and specific energy outflow $\dot{E}_3$ from the growth surface due to the temperature gradient between the condensate and the substrate bottom surface. The specific diffusion flow was determined as $J_d = -D(n - n_0)/\lambda$, where D is the diffusion coefficient of sputtered atoms, n is the current concentration of sputtered atoms above the substrate surface, and λ is the distance between the observation points with concentrations n and n_0.

3. Results and Discussion

3.1. Interrelationships Between Local Growth Kinetics and Local Technological Parameters as a Basis for Pattern Self-Organization

When the deposition process takes place at near thermodynamic equilibrium conditions, mutual interdependence between the growth parameters for adjacent local condensate areas also increases, which is a key factor in the self-assembly of nanopatterned systems. Ostwald ripening can be an illustration of such an self-assembly process. It is common knowledge [50,61–63] that Ostwald ripening, caused by averaging of the nuclei sizes, is possible only provided there is atoms exchange between the nuclei. Based on this,

the nuclei concentration n_c, average size of the nuclei $\bar{r}$, and the average value of atoms mean free path λ_i are interrelated according to the inequality:

$$\left[\pi(\bar{r}+\lambda_i)^2\right]^{-1} < n_c \tag{10}$$

In turn, it follows from [50,61] that the rate of nucleus radius change depends on the radius size r itself according to equation:

$$\frac{dr}{dt} \propto \frac{1}{r^2}\left(\frac{r}{r_c}-1\right), \tag{11}$$

Hence, the critical nucleus radius is $r_c \sim 1/\xi$ [50]; one may conclude that at low values of ξ, during the dissolution of nuclei having dimensions $r < r_c$, the material partially diffuses and then redeposits onto surfaces of larger nuclei that are more resistant to disintegration. Therefore, low supersaturations cause the self-assembly of the nuclei system with radii larger than the critical value, having a uniform shape and size distribution [64,65]. Moreover, the above-described self-organization, when bigger nuclei increase in size at the cost of smaller ones, is based on the mutual exchange of substance between them. It is also worth mentioning that at the beginning instant of the condensation process at low supersaturations, there is an increase in the area of the growth surface, which causes a following reduction of ξ at a constant value of J_s [61] and, as a result, gives rise to an improvement in efficiency of Ostwald ripening self-organization process. Figure 3 represents the stages of self-organization of Cu nanosystems under the conditions of near-equilibrium condensation and the presence of a physically (a, b) [35,64] or chemically (c, d) [65] active medium near the growth surface. The technological setup and condensation parameters have been described in detail in previous works [35,64,65]. In the case of a chemically active medium, the chemical reaction (12) takes place near the surface with the deposition of copper and formation of hydrogen chloride gas. Under conditions close to equilibrium, the working reaction is as follows:

$$CuCl_2 + H_2(gas) \leftrightarrow Cu(s) + 2HCl\ (gas). \tag{12}$$

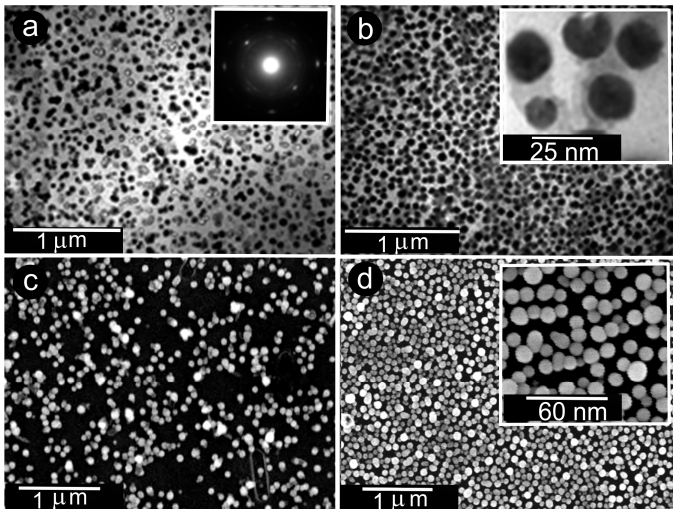


Figure 3. Two stages of sequential growth of copper nanosystems under the action of plasma (**a**,**b**) and under the action of chemically active medium (hydrogen) (**c**,**d**) on the growth surface [35,65].

Low supersaturations accompanied by variations of the electric field strength E over the developed relief of the growing condensate can also have an effect on the self-organization of its particular morphology [66]. The abovementioned self-organization is caused by non-linearly interconnected fluctuations of the chemical potential differences

$\Delta\mu_a$, $\Delta\mu_b$, and $\Delta\mu_c$ determined for adjacent areas a, b, and c of the growing surface that, consequently, are dependent on changes in the electric field intensity and on variations in the morphology of the condensate surface of growth. In this case, the self-organization of the complex developed surface topology was related to the condensate growth rates in the specified three adjacent areas.

The time derivatives $\dot{a}$, $\dot{b}$, and $\dot{c}$ are expressed by the following system of equations [66]:

$$\dot{a} = \frac{2a\Omega_c J_s}{b|a|\pi} - Z_a(\Delta\mu_b, \Delta\mu_c, a, c, b, \gamma_e), \quad (13)$$

$$\dot{b} = \frac{2\Omega_c J_s}{(a+c)\pi} - Z_b(\Delta\mu_a, \Delta\mu_c, a, b, c, \gamma_e), \quad (14)$$

$$\dot{c} = \frac{2c\Omega_c J_s}{|c|\pi(\gamma - b)} - Z_c(\Delta\mu_a, \Delta\mu_b, a, c, b, \gamma_e). \quad (15)$$

At the same time, γ_e is the characteristic size of the growth surface local area on which the self-organization process takes place, and simplified functions $Z_a(\Delta\mu_b, \Delta\mu_c, a, c, b, \gamma_e)$, $Z_b(\Delta\mu_a, \Delta\mu_c, a, b, c, \gamma_e)$ and $Z_c(\Delta\mu_a, \Delta\mu_b, a, c, b, \gamma_e)$ determine the mutual interrelationship between the system parameters, i.e., are the basis of self-organization. The phase portraits, representing solutions of Equations (13)–(15) at different values of E_{eo}, d and J_s and corresponding morphologies of the condensate surface, are presented in Figure 4 [66].

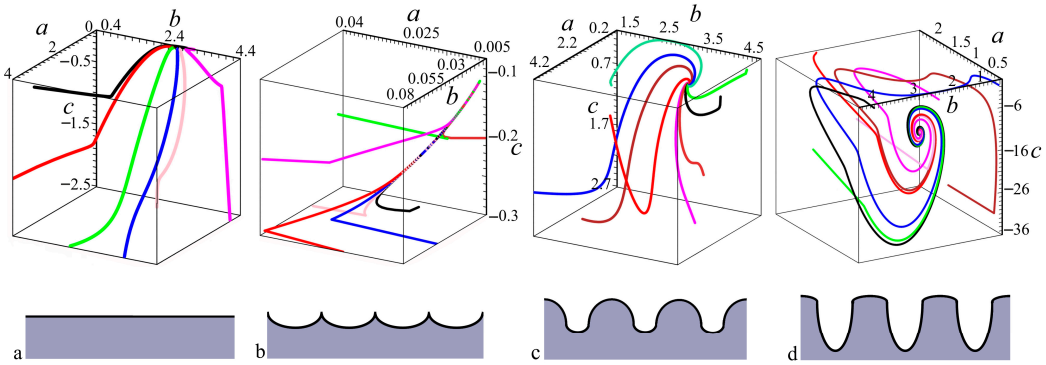


Figure 4. Phase portraits and condensate surface morphologies obtained from the system of Equations (13)–(15) and their solutions at different values of E_{eo}, d and J_s ((**a**)—E_{eo} = 0.001 V/m, J_s = 0.01 m^{-2}s^{-1}, d = 4.1 mm; (**b**)—E_{e0} = 1.0 V/m, J_s = 1.0 m^{-2}s^{-1}, d = 2.1 mm; (**c**)—E_{e0} = 0.24 V/m, J_s = 2.0 m^{-2}s^{-1}, d = 1.5 mm; (**d**)—E_{e0} = 0.24 V/m, J_s = 2.0 m^{-2}s^{-1}, d = 4.1 mm) [66].

Here, E_{e0} is strength of the electric field above the flat growth surface, d is the width of the cathodic potential drop region, and J_s is the flow of the condensing substance. Analyzing the phase portraits, one can come to the conclusion that in the case of the presence of fluctuations of the electric field strength above the condensate growing surface, the self-organization of micro- and nanopatterned structures was observed. Confirmation of such self-organization were the copper and the graphite-like phase morphologies formed under the near-equilibrium conditions implemented in plasma–condensate system and the electrical bias applied to the surface of growth (Figure 5). For the Cu and graphite layers' formation, presented in Figure 2, a technological setup has been implemented; the technological conditions have been described in detail in [41,67].

Under conditions of high supersaturations or at high values of condensing flow J_s, the above-described self-organization process, according to the system of Equations (13)–(15), was not observed. In this case, $\frac{2a\Omega_c J_c}{b|a|\pi} \gg Z_a(\Delta\mu_b, \Delta\mu_c, a, c, b, \gamma_e)$, $\frac{2\Omega_c J_c}{(a+c)\pi} \gg Z_b(\Delta\mu_a, \Delta\mu_c, a, b, c, \gamma_e)$ and $\frac{2c\Omega_c J_c}{|c|\pi(\gamma-b)} \gg Z_c(\Delta\mu_a, \Delta\mu_b, a, c, b, \gamma_e)$, and, as a result, the layer growth rates in three adjacent areas a, b, c did not change over time. Therefore, a necessary prerequisite for the

surface morphology self-organization in the form of patterned micro- and nanosystems is low supersaturation of the condensing vapors.

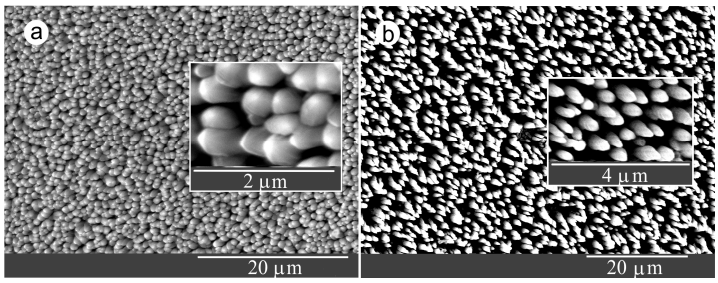


Figure 5. SEM image of the of (**a**) copper and (**b**) graphite condensate morphologies [59].

At the end of this section, it is necessary to point out that the self-organization of patterned micro- and nanosystems is possible not only during condensation under near thermodynamic equilibrium conditions. For example, the transition of a substance from a solid state into a solution, i.e., due to the oxidation of anodes near equilibrium in the electrolyte–condensate system, can also lead to the self-organization effects. Examples of such self-organization include the formation of porous systems of silicon and aluminum [68,69]. In both cases, conducting anodic dissolution in acid-containing electrolytes at high current densities creates the prerequisites for the formation of an ordered system of pores. Moreover, when the current density decreases, the process of chemical interaction with the surface of the anodes (aluminum or silicon) is localized on various active centers. The regularity analysis of ordered pore systems (Figure 6) for anodically oxidized aluminum conducted in [68] indicates that the size of aluminum crystals grain, their crystallographic orientation, and defect density have no pronounced effect on the regularity of the pore arrangement. However, a necessary precondition for ordered and regular pore formation is a high purity of the underlying aluminum, as well as stable in-time anodization parameters such as anodization voltage, electrolyte temperature, and electrolyte concentration.

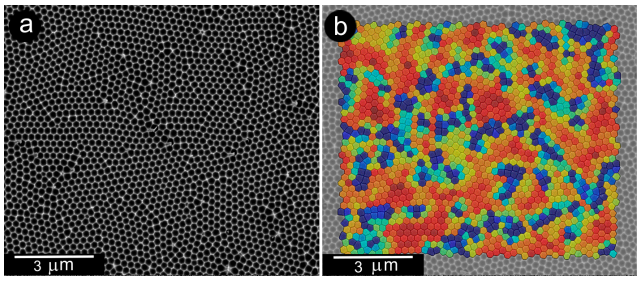


Figure 6. SEM image of anodically oxidized aluminum membrane before (**a**) and after (**b**) its processing using a special program [68].

3.2. Low Supersaturations Dissipative Self-Organization of as a Basis for Nanosystems in the Form of Patterns Formation

Ultra-low supersaturations during deposition from a vapor phase can be achieved by two technological approaches. The first one is based on the condensation of stationary vapor flows J_s, which are maintained by rather high constant temperature T_c and corresponding equilibrium pressure P_e. In addition to that, even with the plasma influence onto the growth surface, for the vast majority of bad-volatile substances, such as metals and semiconductors, negligibly low vapor pressures should be applied with regard to realize near-equilibrium condensation. Apparently, it is very complicated to create weak flows and at the same time to maintain the stationarity of the technological process.

The second method operation principle is based on self-organization of low-supersaturation values in a plasma–condensate system. The required technological conditions were implemented using a technological setup, presented in Figure 2. Taking into account the

interrelation between the process technological parameters, in the work [41], a mathematical model of the dissipative self-organization of low supersaturations was established in the form of the following system of equations:

$$\dot{T}_c = \left(\dot{E}_1 + \dot{E}_2 + \dot{E}_3\right)/c, \tag{16}$$

$$\dot{n} = \frac{\pi}{\delta}\left(\frac{s}{S}J_d - J_s\right), \tag{17}$$

$$\dot{\xi} = \frac{s}{S}\frac{D}{\lambda\delta}\xi_0 - \left(\frac{1}{\tau} + \frac{s}{S}\frac{D}{\lambda\delta}\right)\xi - B(T_c)(1+\xi)T_c, \tag{18}$$

$$\dot{J}_s = \frac{s}{S}\frac{D}{\lambda\tau}n_0 - J_s\left(\frac{1}{\tau} + \frac{s}{S}\frac{D}{\lambda\delta}\right) - \frac{n_e}{\tau}\left(\frac{s}{S}\frac{D}{\lambda} - \delta\cdot B(T_c)\dot{T}_c\right) \tag{19}$$

where c is the growth surface heat capacity; τ is the mean duration of the sputtered atoms motion above the growth surface along a circular path with a mean length of δ; n_e is the equilibrium atoms' concentration; S is the inner cathode surface area; s is the hollow cathode opening area; ξ_0 is the sputtered atoms' relative supersaturation at the inlet to the hollow cathode. It should be mentioned that Equations (16) and (17) are presented in a simplified form, that is, without functional dependencies on the other technological parameters [41].

From the analysis (17), it is easy to show that when the system reaches the stationary regime, i.e., when $\dot{n}_0 = 0$, the diffusion flow J_d and the condensing flow J_s are interrelated according to equation $sJ_d = SJ_s$. This result is quite important for understanding the crucial role of the accumulation of the sputtered substance in the vicinity of the condensate growing surface during small supersaturations self-organization. In this case, the sputtered atoms accumulated near the growth surface until the current pressure P_c of the deposition vapor rise to a certain extent above the equilibrium pressure P_e corresponding to the conditions of low supersaturations. In this case, when the growth surface temperature T_c changed, due to heating caused the plasma action, for example, according to (2), the P_e value rose, and the sputtered atoms kept accumulating even further while retaining small values of supersaturation. In the case of the absence of substance accumulation, similar changes in the growth temperature would cause major transformations in the structure formation mechanisms or even to the termination of the condensation itself. In the self-organized system, the growth of the discharge power led to sequential intensification of the sputtering rate of the target, which was a hollow cathode surface in this case. At the same time, the simultaneous increase in the temperature of the entire hollow cathode took place, indicating, in such a way, that there was an interrelation between the deposition flow and the growth surface temperature. At the same time, the rate of increase in the cathode temperature as a whole depended on its geometry and the material heat capacity. Thus, optimizing the geometry of the cathode, one could fabricate a technological system for a desired material, in which all the main technological parameters are non-linearly interdependent. The above-described peculiarities of the technological setup are a prerequisite for the low supersaturations self-organization and, consequently, for the nanosystems' reproducible synthesis under steady-state condensation conditions without the need to create feedback systems for artificial control of technological process.

Using the system of Equations (16), (18), and (19), a phase portrait was constructed, which was characteristic for silicon as a sputtering material and is shown in Figure 7.

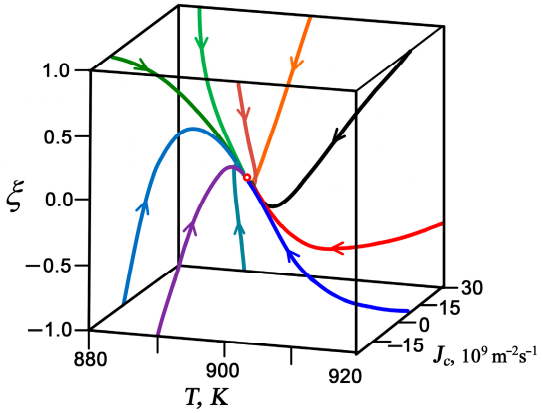


Figure 7. The phase portrait, representing the solution of the system of Equations (16), (18), and (19) for silicon condensation. Different colors represent various initial conditions.

The coordinates of the equilibrium point presented on the phase portrait had the following values: T_c = 898 K, ξ = 4.31·10^{-4}, J_s = 4.31·10^6 (m^{-2}s^{-1}). Along with this, the equilibrium point on the phase portraits with the position evidencing the ultrasmall supersaturations confirmed that the process of dissipative self-organization of the technological conditions was required for a reproducible nanosystem formation. It should also be emphasized that, in this case, nanosystems were formed inside the hollow cathode, which, with some approximation, could be also considered as conservative self-organization. Using sputtering device presented in Figure 6 and varying hollow cathodes geometrical characteristics, micro- and nanostructures of Cu, C, Zn, Al, and Ti were formed (Figure 8). From analysis of obtained porous Al and Ti nanosystems structure and morphology (Figure 8), the conclusion was made that the self-organization of similar crystal habitus can be realized when building crystallographic planes with the maximum density of atoms provided maximally strong chemical bonds are realized during the atoms' condensation. Moreover, the abovementioned fact proves high stationarity the technological process.

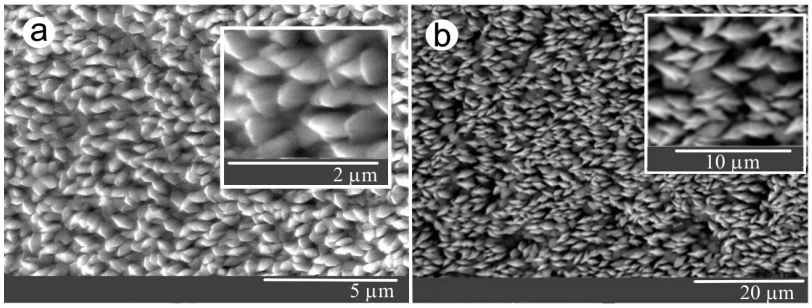


Figure 8. Scanning electron microscopic images of (**a**) Al and (**b**) Ti condensates [59].

Let us consider another example of dissipative functional self-organization implemented in [70–74] during multilayer carbon nanotubes' (MCNTs) formation by means of an arc discharge created between two graphite electrodes in a helium atmosphere. First of all, it is necessary to point out that a rather small distance between the graphite electrodes (~1 mm, [73–76]) was used in this case, which indicates the possibility that carbon atoms evaporated from the anode accumulate near the condensate growing surface. It should also be noted that the closeness of the system was enhanced by the accumulation of positive carbon ions near the substrate, which was located on the cathode side. The physical model of the flow balance and the energy balance is schematically presented in Figure 9. The speed of variation in carbon concentration was determined by the difference of carbon specific flows coming in and coming out of the substance accumulation area and was characterized by the following flows: J_D is the diffusion flow evaporated from the anode 1 and entering the accumulation area 2 focusing onto the cathode surface; J_v is the spe-

cific flow of re-evaporated from the cathode atoms and re-entering the condensation area; J_f is the specific flow of carbon ions directed from the accumulation zone to the MCNTs condensation surface.

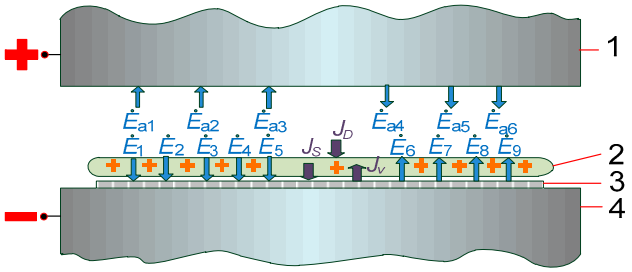


Figure 9. Schematic representation of the physical model of the flow and energy balance between the two graphite electrodes (1—the anode; 2—the carbon ions accumulation area; 3—the condensate in the form of MCNTs; 4—the cathode).

At the cathode surface, the balance of energy was characterized by following factors: $\dot{E}_1$ is the speed of energy input to the surface of growth because of the recombining of adsorbed carbon ions, taking into account the electron work function from the volume to the surface of the MCNTs; $\dot{E}_2$ is the specific energy input to the MCNTs' growth surface due to the absorption of the kinetic energy of the carbon ions; $\dot{E}_3$ is the specific energy flow to the growing surface of MCNTs caused by the heat flow of neutral helium atoms; $\dot{E}_4$ is the specific flow of energy input because of the thermal accommodation of carbon atoms taking into account the condensation latent heat; $\dot{E}_5$ is the specific flow of the energy intake to the growth surface due to heat radiation from the heated anode; $\dot{E}_6$ is the specific flow of energy output from the MCNRs' growth surface due to the desorption of carbon atoms; $\dot{E}_7$ is the specific flow of energy output from the MCNTs' growth surface because of the thermal emission of electrons; $\dot{E}_8$ is the specific flow of energy output to a cooler from the MCNTs' growth surface due to the cathode material thermal conductivity; $\dot{E}_9$ is the specific flow of energy by means of thermal radiation out of the growth surface.

The energy balance at the anode surface was determined by following factors: $\dot{E}_{a1}$ is the specific flow of energy input to the surface due to the bombardment of plasma electrons; $\dot{E}_{a2}$ is the specific flow of energy input to the surface due to the action of the flow of neutral helium atoms; $\dot{E}_{a3}$ is the specific flow of energy intake because of thermal radiation from the heated cathode; $\dot{E}_{a4}$ is the specific flow of energy output due to carbon atoms evaporation of from the anode; $\dot{E}_{a5}$ is the specific flow of energy outcome due to the heat removal from the anode toward the cooler; $\dot{E}_{a6}$ is the specific flow of energy outcome by means of anode surface thermal radiation.

Based on the analysis of the physical model a corresponding mathematical model was built [42], which consists of the following system of differential equations:

$$\dot{n} = \left(J_D + J_v + J_f\right)/h, \tag{20}$$

$$\dot{T}_c = \frac{1}{c_{dep}} \sum_{i=1}^{6} \dot{E}_i, \tag{21}$$

$$\dot{T}_a = \frac{1}{c_a} \sum_{i=1}^{9} \dot{E}_{ai}, \tag{22}$$

$$\dot{\xi} = \left(\dot{n}\, n_e - n\dot{n}_e\right)/n_e^2 \tag{23}$$

Here, h—the characteristic size of carbon atoms accumulation area; $\dot{n}$—the concentration change rate of carbon atoms in the accumulation area; c_{dep}—the heat capacity of the MCNTs surface layer grown on the cathode surface; n_e—the equilibrium concentration of carbon atoms in the accumulation area or above the MCNTs' growth surface.

In the work [42], relations that determine the dependence of the system parameters in Equations (20)–(23) on the plasma arc discharge characteristics were determined together with regularities of the plasma interaction with the anode surface and the MWCNs growth surface. Moreover, the physical foundations of the carbon atoms' evaporation from the anode, thermal radiation from the cathode and the anode, as well as diffusion movement and technological parameters of condensation of carbon atoms in the form of MCNTs on the cathode, were established. Equations (20)–(22) determine the flow balance of carbon atoms evaporated from the anode and directed to the accumulation area together with the energy balances at the cathode and anode surfaces. At the same time, Equation (23) is a derivative of Equation (1), and the analysis of all equations indicates a direct or indirect mutual interrelationship between the main parameters of the equations system, which is a prerequisite for the self-organization of technological conditions necessary for the formation of MCNTs. Evidence of such self-organization is the presence of equilibrium points on the phase portraits built on the basis of the system of Equations (20)–(22) (see Figure 10a) and the system of Equations (21)–(23) (see Figure 10b) [42].

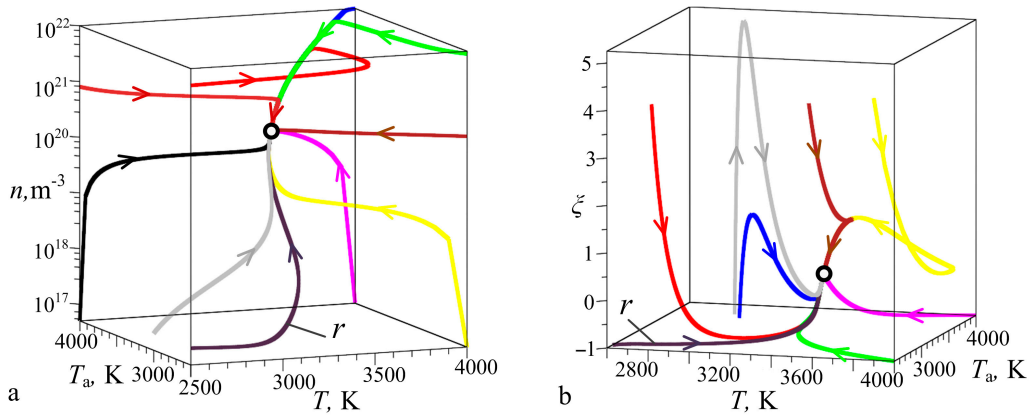


Figure 10. Phase portraits of the system of Equations (20)–(22) (**a**) and Equations (21)–(23) (**b**) [42].

Coordinates of the equilibrium points on the phase portraits (T = 3363 K, T_a = 3569 K, $n = 1.4110^{20}$ m^{-3}, $\xi = 3.0810^{-2}$) confirmed the necessary prerequisites for the formation of MCNTs, which were determined by the ultralow stationary values of relative supersaturation. At the same time, we can talk about the spatially distributed selectivity of the MCNTs' formation on the cathode surface during the accumulation of carbon plasma in a certain volume, which had signs of conservative self-organization. Therefore, in the described examples of small supersaturations' dissipative self-organization, there were indications of conservative self-organization of patterned micro- and nanosystems. Therefore, one can make conclusions about the integration of dissipative and conservative self-organizations within the framework of a system of complete self-organization. A schematic representation of interconnections in such system implemented based on the hollow cathode (Figure 2) is presented in Figure 11. At the same time, the green arrows on the schematic image indicate direct and inverse relationships between all system parameters, which is the basis of the nanotechnological process complete self-organization.

In conclusion, it should be emphasized that the most important operation peculiarity of completely self-organized systems is the presence of structure formation zones within each one variation in deposition parameters, such as the pressure of the working gas or the applied power of discharge, has no effect on the structure and morphology of the resultant micro- and nanosystems. This assumption has been confirmed when obtaining MCNTs in

the arc discharge between two graphite electrodes [70–74], as well as when obtaining zinc nanosystems in the device with a hollow cathode (Figure 2). Moreover, similar variations in technological process parameters without the involvement of self-organization would inevitably cause considerable deviations in the condensate formation kinetics.

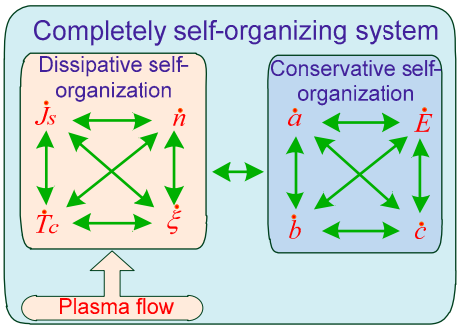


Figure 11. Schematic representation of a completely self-organized system, implemented in a device based on a hollow cathode (Figure 2).

4. Conclusions

1. Self-organization of micro- and nanosystems in the form of patterns at condensate formation from a vapor phase could be realized under the condition of small supersaturation and the presence of a limited number of active centers on the growing surface. Along with this, the influence of the plasma onto the condensate surface reduced the desorption energy of adatoms to an effective value, which made it possible to increase the vapor flow of the condensed substance, keeping the value of the relative supersaturations small and steady.
2. The reproducible formation of patterned micro- and nanosystems was possible under the condition of stationary quasi-equilibrium condensation. The criterion of stationarity was defined by the time-invariant critical desorption energy value or its constant position in the spectrum of all possible desorption energies.
3. When the condensation conditions approached thermodynamic equilibrium, the local condensate growth kinetics and the corresponding local deposition parameters became interdependent. This interdependence was a precondition for self-organization of patterned micro- and nanosystems in different structural and morphological forms. Moreover, the processes of the condensates self-organization could be also affected by the fluctuations in the electrical voltages above the growth surface.
4. The self-organization of patterns occurred according to the principles of conservative self-organization, i.e., at extremely low relative supersaturations in the vapor accumulation volume due to relatively weak diffusion flows. Thus, the combination of dissipative self-organization of small supersaturations with a conservative self-organization of patterned micro- and nanosystem in different structural and morphological forms represents a system of complete self-organization.

Author Contributions: Conceptualization, V.P., A.K. and Y.K.; methodology, V.P.; software, Y.K.; validation, V.P., A.K. and Y.K.; formal analysis, A.K. and Y.K.; investigation, V.P., A.K. and Y.K.; resources, M.K.; data curation, V.P. and G.W.; writing—original draft preparation, V.P., A.K. and Y.K.; writing—review and editing, V.P. and G.W.; visualization, Y.K. and M.K.; supervision, V.P. and G.W.; project administration, V.P.; funding acquisition, V.P. and A.K. All authors have read and agreed to the published version of the manuscript.

Funding: This research received no external funding.

Data Availability Statement: The original contributions presented in the study are included in the article material; further inquiries can be directed to the corresponding author.

Acknowledgments: Anna Kornyushchenko thanks Philipp Schwartz Initiative of the Alexander von Humboldt Foundation for supporting her research topic and giving scholarship that allowed her to continue research work at Institute of Materials Physics, University of Münster, Germany.

Conflicts of Interest: The authors declare no conflicts of interest.

References

1. Kwon, H.; Alarcón-Correa, M.; Schärf, I.; Fischer, P. Ultrathin nanoporous metallic films and their integration in sensors. *Mater. Adv.* **2024**, *5*, 3973–3980. [CrossRef]
2. Chu, Y.; Zhou, H.; Wang, X.; Zhang, H.; Zhao, L.; Xu, T.; Yan, H.; Zhao, F. A flexible and self-supported nanoporous gold wire electrode with a seamless structure for electrochemical ascorbic acid sensor. *Microchem. J.* **2023**, *186*, 108259. [CrossRef]
3. Si, L.; Yu, P.; Huang, J.; Zhao, Z.; Huang, M.; He, S.; Liu, H.; Wang, X.; Liu, W. Advances in gas-sensitive materials based on polyurethane film, foam, and fiber. *Mater. Today Commun.* **2024**, *38*, 108528. [CrossRef]
4. Kim, H.J.; Lee, J.H.; Jeon, J.G.; Shin, G.; So, B.J.; Choi, Y.; Lee, H.; Kim, J.H.; Kang, T.J. Overpotential-controlled deposition of porous platinum for non-enzymatic glucose detection. *Microchem. J.* **2024**, *204*, 111113. [CrossRef]
5. Zhang, J.; Xiong, Q.; Xu, J. Research progress in non-precious metal oxide/compound-based electrodes for non-enzymatic electrochemical glucose sensor applications. *Mat. Sci. Semicon. Proc.* **2024**, *181*, 108643. [CrossRef]
6. Mushahary, N.; Sarkar, A.; Basumatary, F.; Brahma, S.; Das, B.; Basumatary, S. Recent developments on graphene oxide and its composite materials: From fundamentals to applications in biodiesel synthesis, adsorption, photocatalysis, supercapacitors, sensors, and antimicrobial activity. *Results Surf. Interfaces* **2024**, *15*, 100225. [CrossRef]
7. Ambi, R.R.; Mane, A.A.; Patil, V.B.; Mane, R.D. Highly porous hierarchical NiO coated ZnO pn heterostructure for NO_2 detection. *MSEB* **2024**, *300*, 117066. [CrossRef]
8. Kadja, G.T.; Ilmi, M.M.; Azhari, N.J.; Khalil, M.; Fajar, A.T.; Makertihartha, I.G.B.N.; Gunawan, M.L.; Rasrendra, C.B.; Wenten, I.G. Recent advances on the nanoporous catalysts for the generation of renewable fuels. *J. Mater. Res. Technol.* **2022**, *17*, 3277–3336. [CrossRef]
9. Tran, D.T.; Van, H.T.; Nguyen, L.H.; Van Quang, N.; Tsai, Y.C.; Lin, K.Y.A.; Tuan, D.D. Hierarchical porous cobalt nanoparticles encapsulated in heteroatom-doped hollow carbon as an enhancing multifunctional catalyst for hydrolysis of sodium borohydride and hydrogenation of bromate in water. *J. Surf. Interfaces* **2024**, *48*, 104329. [CrossRef]
10. Kadja, G.T.; Mardiana, S.; Culsum, N.T.; Saputera, W.H.; Azhari, N.J.; Krisnandi, Y.K.; Khatrin, I.; Pamungkas, A.Z.; Larasati, L.; Lestari, W.W.; et al. Recent advances in the synthesis of hierarchically porous catalysts for the generation of renewable fuels. In *Comprehensive Materials Processing*, 2nd ed.; Hashmi, S., Ed.; Elsevier: Amsterdam, The Netherlands, 2024; Volume 2, pp. 249–263. [CrossRef]
11. Mondal, K.; Malode, S.J.; Shetti, N.P.; Alqarni, S.A.; Pandiaraj, S.; Alodhayb, A. Porous nanostructures for hydrogen generation and storage. *J. Energy Storage* **2024**, *76*, 109719. [CrossRef]
12. Goc, K.; Prendota, W.; Przewoźnik, J.; Gondek, Ł.; Kapusta, C.; Radziszewska, A.; Mineo, K.; Takasaki, A. Magnetron sputtering as a method for introducing catalytic elements to magnesium hydride. *Int. J. Hydrogen Energy* **2018**, *43*, 20836–20842. [CrossRef]
13. Li, L.; Deng, Y.; Hu, K.; Xu, B.; Wang, N.; Bai, Z.; Xu, X.; Yang, J. Nanostructure designing and hybridizing of high-capacity silicon-based anodes for lithium-ion batteries. *Prog. Nat. Sci.-Mater.* **2023**, *33*, 16–36. [CrossRef]
14. Darjazi, H.; Madinabeitia, I.; Zarrabeitia, M.; Gonzalo, E.; Acebedo, B.; Javad Rezvani, S.; Fernández-Carretero, F.J.; Nobili, F.; García-Luis, A.; Muñoz-Márquez, M.Á. $LiNi_{0.5}Mn_{1.5}O_4$ thin films grown by magnetron sputtering under inert gas flow mixtures as high-voltage cathode materials for lithium-ion batteries. *Chem. Electro. Chem.* **2023**, *10*, e202201004. [CrossRef]
15. Li, Y.; Chen, Q.; Meng, Q.; Lei, S.; Song, F.; Ma, J. Synergy of a hierarchical porous morphology and anionic defects of nanosized $Li_4Ti_5O_{12}$ toward a high-rate and large-capacity lithium-ion battery. *J. Energy Chem.* **2021**, *54*, 699–711. [CrossRef]
16. Cao, Z.; Yang, Y.; Qin, J.; Su, J. A core-shell porous MnO_2/Carbon nanosphere composite as the anode of lithium-ion batteries. *J. Power Sources* **2021**, *491*, 229577. [CrossRef]
17. Li, Y.; Yan, Y.; Yao, M.S.; Wang, F.; Li, Y.; Collins, S.M.; Du, S. Porous electrodes from self-assembled 3D jointed Pd polyhedra for direct formic acid fuel cells. *Chem. Eng. J.* **2023**, *462*, 142244. [CrossRef]
18. Zhang, Y.; Tao, Y.; Shao, J. Application of porous materials for the flow field in polymer electrolyte membrane fuel cells. *J. Power Sources* **2021**, *492*, 229664. [CrossRef]
19. Wiame, F. Strategies for the growth of large-scale self-organized structures. *Thin Solid Film.* **2017**, *642*, 258–275. [CrossRef]
20. Desai, R.C.; Kapral, R. *Dynamics of Self-Organized and Self-Assembled Structures*; Cambridge University Press: Cambridge, UK, 2009.
21. Haken, H. *Information and Self-Organization*; Springer: Berlin, Germany, 2000.
22. Haken, H. Synergetics. In *Introduction and Advanced Topics*; Springer: Berlin/Heidelberg, Germany; New York, NY, USA, 2004.
23. Eessaa, A.K.; El-Shamy, A.M. Review on fabrication, characterization, and applications of porous anodic aluminum oxide films with tunable pore sizes for emerging technologies. *Microelectron. Eng.* **2023**, *279*, 112061. [CrossRef]
24. Prigogine, I.; Nicolis, G. *Self-Organization in Non-Equilibrium Systems*; Wiley: New York, NY, USA, 1977.
25. Al-Shamery, K.; Parisi, J. (Eds.) *Self-Organized Morphology in Nanostructured Materials*; Springer: Berlin, Germany, 2007.
26. Müller, I.; Weiss, W. Thermodynamics of irreversible processes—Past and present. *Eur. Phys. J. H* **2012**, *37*, 139–236. [CrossRef]

27. Ivanova, V.S.; Balankin, A.S.; Bunin, I.Z.; Oksogoev, A.A. *Synergetics and Fractals in Materials Science*; Nauka: Moscow, Russia, 1994.
28. Ivanova, V.S.; Bunin, I.J.; Nosenko, V.I. Fractal material science: A new direction in materials science. *JOM* **1998**, *50*, 52–54. [CrossRef]
29. Olemskoi, A.I.; Khomenko, A.V. *Synergetics of Condensed Matter: A Textbook for University Students*; Sumy State University: Sumy, Ukraine, 2002. (In Russian)
30. Müller, A.; Reuter, H.; Dillinger, S. Supramolecular Inorganic Chemistry: Small Guests in Small and Large Hosts. *Angew. Chem. Int. Ed. Engl.* **1995**, *34*, 2328–2361. [CrossRef]
31. Adachi, M.; Lockwood, D.J. *Self-Organized Nanoscale Materials*; Springer: Berlin, Germany, 2006.
32. Lehn, J.M.; Sanders, J.K.M. Supramolecular Chemistry: Concepts and Perspectives. *Angew. Chem. Int. Ed. Engl.* **1995**, *34*, 2563. [CrossRef]
33. Pearce, N.; Champness, N.R. *Metal Complexes in Supramolecular Chemistry and Self-Assembly. Reference Module in Chemistry, Molecular Sciences and Chemical Engineering*; Elsevier: Amsterdam, The Netherlands, 2020. [CrossRef]
34. Müller, S.C.; Parisi, J. *Bottom-Up Self-Organization in Supramolecular Soft Matter*; Springer: Berlin, Germany, 2015. [CrossRef]
35. Perekrestov, V.I.; Kornyushchenko, A.S.; Kosminskaya, Y.A. Formation of nanosystems under near-equilibrium copper condensation in an ultrapure inert medium. *JETP Lett.* **2008**, *86*, 767–771. [CrossRef]
36. Perekrestov, V.I.; Kosminska, Y.O.; Kornyushchenko, A.S.; Mokrenko, A.A. Impact of selective processes on Al porous structures formation during self-organized quasi-equilibrium steady-state condensation. *J. Porous Mater.* **2013**, *20*, 967–974. [CrossRef]
37. Halley, J.D.; Winkler, D.A. Consistent concepts of self-organization and self-assembly. *Complexity* **2008**, *14*, 10–17. [CrossRef]
38. Chernov, A.A. *Modern Crystallography III: Crystal Growth*; Springer: Berlin, Germany, 2012.
39. Martin, P.M. *Handbook of Deposition Technologies for Films and Coatings: Science, Applications and Technology*; William Andrew: Oxford, UK, 2009.
40. Perekrestov, V.I.; Kosminska, Y.O.; Mokrenko, A.A.; Kononenko, I.N.; Kornyushchenko, A.S. Structure formation mechanisms of low-dimensional porous titanium systems condensed under quasi-equilibrium steady-state conditions. *Vacuum* **2011**, *86*, 111–118. [CrossRef]
41. Perekrestov, V.I.; Olemskoi, A.I.; Kosminska, Y.O.; Mokrenko, A.A. Self-organization of quasi-equilibrium steady-state condensation in accumulative ion-plasma devices. *Phys. Lett. A* **2009**, *373*, 3386–3391. [CrossRef]
42. Kosminska, Y.O.; Perekrestov, V.I. Regularities of self-organization of technological conditions during plasma-arc synthesis of carbon nanotubes. *Diam. Relat. Mater.* **2018**, *85*, 37–48. [CrossRef]
43. Harsha, K.S. *Principles of Physical Vapor Deposition of Thin Films*; Elsevier: Oxford, UK, 2006.
44. Kelly, P.J.; Arnell, R.D. Magnetron sputtering: A review of recent developments and applications. *Vacuum* **2000**, *56*, 159–172. [CrossRef]
45. Greene, J.E. Tracing the recorded history of thin-film sputter deposition: From the 1800s to 2017. *J. Vac. Sci. Technol. A* **2017**, *35*, 05C204. [CrossRef]
46. Konuma, M. *Film Deposition by Plasma Techniques*; Springer: Berlin, Germany, 2012.
47. Randhawa, H. Review of plasma-assisted deposition processes. *Thin Solid Film.* **1991**, *196*, 329–349. [CrossRef]
48. Rollings, E.; Gweon, G.-H.; Zhou, S.Y.; Mun, B.S.; McChesney, J.L.; Hussain, B.S.; Fedorov, A.V.; First, P.N.; de Heer, W.A.; Lanzara, A. Synthesis and characterization of atomically thin graphite films on a silicon carbide substrate. *J. Phys. Chem. Solids* **2006**, *67*, 2172–2177. [CrossRef]
49. Hass, J.; Feng, R.; Li, T.; Li, X.; Zong, Z.; de Heer, W.A.; First, P.N.; Conrad, E.H.; Jeffrey, C.A.; Berger, C. Highly ordered graphene for two dimensional electronics. *Appl. Phys. Lett.* **2006**, *89*, 143106. [CrossRef]
50. Kukushkin, S.A.; Osipov, A.V. Thin-film condensation processes. *Phys. Usp.* **1998**, *41*, 983. [CrossRef]
51. Birney, R. Special Issue: Current Research in Thin Film Deposition: Applications, Theory, Processing, and Characterization. *Coatings* **2020**, *10*, 1228. [CrossRef]
52. Walgraef, D. Nanostructure evolution during thin film deposition. *Phys. E Low-Dimens. Syst. Nanostruct.* **2003**, *18*, 393–401. [CrossRef]
53. Du, D.; Srolovitz, D.J. Crystal morphology evolution in film growth: A general approach. *J. Cryst. Growth* **2006**, *96*, 86–96. [CrossRef]
54. Kukushkin, S.A.; Osipov, A.V. New phase formation on solid surfaces and thin film condensation. *Prog. Surf. Sci.* **1996**, *51*, 1–107. [CrossRef]
55. Osipov, A.V. Kinetic model of vapour-deposited thin film condensation: Nucleation stage. *Thin Solid Film.* **1993**, *227*, 111–118. [CrossRef]
56. Dubrovskii, V.G.; Cirlin, G.E. Growth kinetics of thin films formed by nucleation during layer formation. *Semiconductors* **2005**, *39*, 1267–1274. [CrossRef]
57. Kuni, F.M.; Shchekin, A.K.; Grinin, F.P. Theory of heterogeneous nucleation under conditions of gradual formation of a metastable state. *Usp. Fiz. Nauk* **2001**, *171*, 345–385. [CrossRef]
58. Pedersen, H.; Elliott, S.D. Studying chemical vapor deposition processes with theoretical chemistry. *Theor. Chem. Acc.* **2014**, *133*, 1476. [CrossRef]

59. Perekrestov, V.I.; Kornyushchenko, A.S.; Kosminska, Y.A.; Shevchenko, S.T.; Natalich, V.V. Systems of complete self-organization of the nanotechnological process. In Proceedings of the 2021 IEEE 11th International Conference Nanomaterials: Applications & Properties (NAP), Odessa, Ukraine, 5–11 September 2021; pp. NSS09-1–NSS09-4. [CrossRef]
60. Perekrestov, V.I.; Mokrenko, A.A.; Kosminskaya, Y.A.; Rubets, D.I. Formation of Nickel Extended Surface upon Quasi-Equilibrium Steady-State Condensation. *J. Surf. Investig. Synchrotron Neutron Tech.* **2011**, *5*, 667–671. [CrossRef]
61. Dubrovsky, V.G. Criterion for the onset of the Ostwald ripening stage, taking into account fluctuations in the number of particles in the bud. *Tech. Phys. Lett.* **2010**, *36*, 219–223. [CrossRef]
62. Galdikas, A. Study of nanoclusters growth at initial stages of ultrathin film deposition by kinetic modeling. *Appl. Surf. Sci.* **2008**, *254*, 3964–3970. [CrossRef]
63. Bunshah, R. *Handbook of Deposition Technologies for Films and Coatings: Science, Technology and Applications*; Noyes Publications: New York, NY, USA, 1994.
64. Perekrestov, V.I.; Kosminska, Y.O.; Kornyushchenko, A.S.; Latyshev, V.M. Self-assembly of porous Cu structures during steady-state condensation of weakly supersaturated vapors. *J. Porous Mater.* **2014**, *21*, 1159–1167. [CrossRef]
65. Kornyushchenko, A.S.; Natalich, V.V.; Perekrestov, V.I. Formation of copper porous structures under near-equilibrium chemical vapor deposition. *J. Cryst. Growth* **2016**, *442*, 68–74. [CrossRef]
66. Perekrestov, V.I.; Kosminska, Y.O.; Mokrenko, A.A.; Davydenko, T. Self-assembly of condensates with advanced surface by means of the competing field selectivity and Gibbs–Thomson effect. *Appl. Surf. Sci.* **2014**, *298*, 171–175. [CrossRef]
67. Kornyushchenko, A.S.; Natalich, V.V.; Shevchenko, S.T. Selective processes during formation of porous carbon nanosystems. In Proceedings of the 2019 IEEE 9th International Conference Nanomaterials: Applications & Properties (NAP), Odessa, Ukraine, 15–20 September 2019; pp. 01SSAN20-1–01SSAN20-4. [CrossRef]
68. Ostendorp, S. Anodic Aluminum Oxide for Surface Nano-Structuring Purposes. Ph.D. Thesis, Muenster University, Münster, Germany, 2017.
69. Granitzer, P.; Rumpf, K. Porous silicon—A versatile host material. *Materials* **2010**, *3*, 943–998. [CrossRef]
70. Levchenko, I.; Keidar, M.; Xu, S.; Kersten, H.; Ostrikov, K. Low-temperature plasmas in carbon nanostructure synthesis. *J. Vac. Sci. Technol. B* **2013**, *31*, 050801. [CrossRef]
71. Prasek, J.; Drbohlavova, J.; Chomoucka, J.; Hubalek, J.; Jasek, O.; Adam, V.; Kizek, R. Methods for carbon nanotubes synthesis—A review. *J. Mater. Chem.* **2011**, *21*, 15872–15884. [CrossRef]
72. Iijima, S. Helical microtubules of graphitic carbon. *Nature* **1991**, *354*, 56–58. [CrossRef]
73. Gershman, S.; Raitses, Y. Unstable behavior of anodic arc discharge for synthesis of nanomaterials. *J. Phys. D Appl. Phys.* **2016**, *49*, 345201. [CrossRef]
74. Yeh, Y.W.; Raitses, Y.; Yao, N. Structural variations of the cathode deposit in the carbon arc. *Carbon* **2016**, *105*, 490–495. [CrossRef]
75. Ng, J.; Raitses, Y. Self-organization processes in the carbon arc for nanosynthesis. *J. Appl. Phys.* **2015**, *117*, 063303. [CrossRef]
76. Shashurin, A.; Keidar, M. Factors affecting the size and deposition rate of the cathode deposit in an anodic arc used to produce carbon nanotubes. *Carbon* **2008**, *46*, 1826–1828. [CrossRef]

Disclaimer/Publisher's Note: The statements, opinions and data contained in all publications are solely those of the individual author(s) and contributor(s) and not of MDPI and/or the editor(s). MDPI and/or the editor(s) disclaim responsibility for any injury to people or property resulting from any ideas, methods, instructions or products referred to in the content.